applied sciences

MDPI

Article

# Electrochemical Detection of Chloride Ions by Copper (II) Complex with Mixed Ligand of Oxindole Derivative and Dithiocarbamates Moiety

**M. Nazim [1,†], Abdullah [1,†], Sadia Ameen [2,*], M. Shaheer Akhtar [3] and Hyung-Shik Shin [1,*]**

[1] Energy Materials & Surface Science Laboratory, Solar Energy Research Center, School of Chemical Engineering, Chonbuk National University, Jeonju 54896, Korea; nazim@jbnu.ac.kr (M.N.); abdullahazmi@jbnu.ac.kr (A.)

[2] Advanced Materials and Devices Laboratory, Jeongeup Industry-Academic Cooperation Support Centre, Jeongeup Campus, Chonbuk National University, Jeongeup 56212, Korea

[3] New & Renewable Energy Material Development Center (NewREC), Chonbuk National University, Jeonbuk 56332, Korea; shaheerakhtar@jbnu.ac.kr

* Correspondence: sadiaameen@jbnu.ac.kr (S.A.); hsshin@jbnu.ac.kr (H.-S.S.)

† Authors are equally contributed in this work.

Received: 16 January 2019; Accepted: 22 March 2019; Published: 31 March 2019


**Abstract:** The present work describes the synthesis of a new copper (II) complex with bidentate ligands based on oxindole (indolin-2-one) derivatives, namely: 1*H*,1′*H*,1″*H*-[2,3′:2′,3″-terbenzo[*b*]pyrrol]-2″(3″*H*)-one (L1) and [sodium diethyldithiocarbamate (DTC)] (L2) as a second bidentate ligand. The ligand L1 was prepared by the cyclization reaction of oxindole (2-indolone) with phosphorus oxychloride. A mixed-ligand was synthesized using L1 and L2 ligands with copper (Cu (II)) via a simple reflux process. The synthesized mixed Cu (II) complex [$C_{53}H_{44}CuN_7O_4S_2$ and $[Cu(L1)_2(L2)]2H_2O$] exhibited superior solubility in organic solvents like dichloromethane, chloroform, ethanol, methanol, DMF and DMSO. The optical characterizations revealed that the synthesized Cu (II) complex displayed a broad band ($^2E_g \rightarrow {}^2T_{2g}$) with the absorption at ~420 nm, suggesting a distorted octahedral geometry due to the strong Jahn-Teller distortion of the $Cu^{2+}$ ion. The elemental analysis confirmed the existence of Cu, C, S, N, and other elements in the synthesized mixed Cu (II) complex. The physicochemical studies of the organic ligand and Cu(II) complex were investigated by TG analysis, NMR, FTIR, SEM, EDX, electronic spectra and cyclic voltammetry measurements. The detection of chloride ions with the prepared mixed Cu(II) complex was studied by cyclic voltammetry measurements at different scan rates.

**Keywords:** bidentate ligand; oxindole; sodium diethyldithiocarbamate; spectroscopic studies; chloride ion detection

## 1. Introduction

Various symmetrical and unsymmetrical multidentate organic ligands have played a crucial part in designing metal complexes via coordination with different metal ions [1]. The versatile design of various metal complexes has been observed due to their diverse oxidation states and coordination properties [2,3]. The metal complexes have been widely used as drugs and diagnostic agents because they have shown easy interactions with different biomolecules and hence contributed to the development of new therapeutic or diagnostic agents [4,5]. In various biological systems, copper shows many spectral and chemical properties due to the presence of different organic ligands in the coordination sphere [6]. The novel oxindole derivatives have been extensively explored and investigated for various biological applications [7,8]. The cyclization reaction of various

oxindole-derivatives is applied to the construction of C-C bonds [9–12]. The functionalization of various C-H bonds of oxindole-derivatives has been reported as oxidative coupling of C-H bonds, Heck reaction, etc. for economical and elegant applications [13–16]. Various transition metal complexes have been explored in several applications as optoelectronics [17,18], semiconductors [19], biochemistry [20] and sensors for polymer membranes [21–23]. However, the nitrogen-containing macrocycles exhibit high affinity towards metal ions for coordination [24].

In this study, the synthesis and various spectroscopic studies were performed for a novel mixed Cu (II) complex: the as-synthesized organic ligand named 1*H*,1′*H*,1″*H*-[2,3′:2′,3″-terbenzo[*b*]pyrrol]-2″(3″*H*)-one (L1) and the well-known diethyldithiocarbamate (DTC) ligand (L2) mixed with copper (II) chloride dihydrate (2:1:1 ratio) in methanol solvent to produce the target Cu (II) complex. The electrochemical investigation of the novel Cu (II) complex was studied by cyclic voltammetry (CV) in a three-electrode system by using tetrabutylammonium hexafluorophosphate ($TBAPF_6$) as a supporting electrolyte. The prepared Cu (II) complex was utilized as electrode materials for the electrochemical detection of chloride ions ($Cl^-$) using NaCl (10 µL, 0.1 M) in a standard buffer solution (pH = 7) with different scan rates.

## 2. Materials and Methods

### *2.1. Materials and Methods*

All reagents and chemicals were of analytical grade and used as received unless otherwise noted. The obtained metal complex was purified by recrystallization in hexane. The sodium diethyldithiocarbamate (L2) and Cu (II) chloride dihydrate were obtained from Sigma-Aldrich, St. Louis, Missouri, United States.

### *2.2. Characterizations*

The optical properties of the synthesized complex were studied by ultraviolet-visible (UV–Vis) spectroscopy (V-670, JASCO spectrophotometer, Japan) at room temperature. To identify the various phases of solid material, X-ray powder diffraction (XRD, Rigaku, Cu Kα, λ = 1.54178 Å, Tokyo, Japan) was applied in the Bragg angle range of ~10° and ~80°. The nature of the various chemical bonds and functional groups were investigated by Fourier transform infrared (FTIR, Nicolet, IR300 Thermo Fisher Scientific, Waltham, MA, USA) spectra and elemental analysis (EA Thermal analyzer, Thermo Fisher Scientific, Waltham, MA, USA). Field emission scanning electron microscopy (FESEM, Hitachi 4800, Tokyo, Japan) was used for morphology, and energy-dispersive X-ray (EDX) spectroscopy coupled with FESEM was applied to determine the elemental analysis. Cyclic voltammetry (CV) was used to find out the oxidation states and redox behavior of the Cu (II) complex by using WPG 100 Potentiostat/Galvanostat (WonATech, Seoul, Korea). In the three-electrode system, the CV experiments were executed in 0.1 M tetrabutyl ammonium hexafluorophosphate ($TBAPF_6$) as supporting electrolytes an acetonitrile solution with ferrocene as an internal reference. The metal complex deposited on glassy carbon (GCE) was used as a working electrode, and a saturated calomel reference electrode (SCE) and a platinum wire as a counter electrode at ~100 mV/s scan rate during the experiment.

### *2.3. Synthesis of Ligand*

The heterocyclic organic ligand (L1) was synthesized by a single-step cyclization condensation reaction from oxindole in the presence of $POCl_3$ at reflux temperature [25]. The Cu (II) complex (Scheme 1) was synthesized using $CuCl_2 \cdot 2H_2O$ as the precursor and sodium diethyldithiocarbamate as a secondary ligand (L2). The structures of both the ligands and their Cu (II) complex (Figure 1) were characterized by the various spectroscopic studies.

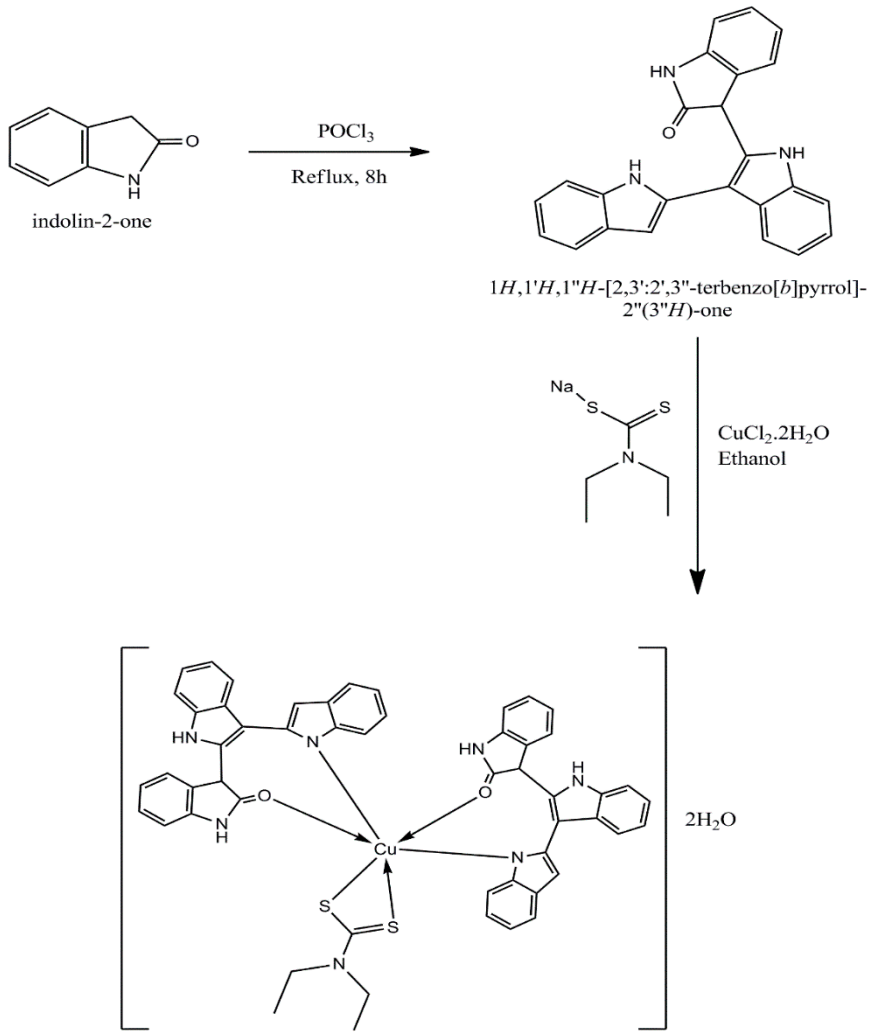


**Scheme 1.** Synthesis of mixed-ligand Cu (II) complex of oxindole-based organic ligand (L1) and dithiocarbamate (L2).

2.3.1. Synthesis of Organic Ligand (1*H*,1′*H*,1″*H*-[2,3′:2′,3″-terbenzo[*b*]pyrrol]-2″(3″*H*)-one) (L1)

The oxindole (1.0 g, 7.5 mmol) and $POCl_3$ (10 mL) were added into a round bottom flask and then refluxed for 8 h under an inert atmosphere. After completion, the reaction was cooled to room temperature and poured into ice water followed by dropwise addition of KOH solution (aq.) to adjust the pH of the reaction mixture. The brown precipitate obtained was filtered, dried and purified by silica gel column (hexane:dichloromethane, 1:1) chromatography to get L1 (30% yield). Scheme 2 shows the electron delocalization behavior via keto-enol equilibrium in the ligand (L1) $^1$H NMR (400 MHz, DMSO, ppm): δ 8.75 (s, 1H), 8.42 (s, 1H), 8.22 (d, 2H), 8.10 (d, 2H), 8.00 (s, 1H), 7.80 (1H), 7.76 (dd, 2H), 7.63 (m, 2H), 7.44 (m, 1H), 7.00 (m, 1H), 6.85 (m, 2H), 6.61 (1H); IR (KBr, $cm^{-1}$): 3421, 3244, 3057, 2920, 2853, 1629, 1469, 1422, 1373, 1328, 1275, 1248, 1078, 1011, 917, 837, 774, 748, 730. Elemental analysis for $C_{24}H_{17}N_3O$ is calculated as: 79.31% (carbon), 4.72% (hydrogen), 11.56% (nitrogen), 4.40% (oxygen); Found: 79.68% (carbon), 4.86% (hydrogen), 11.23% (nitrogen), 4.23% (oxygen).

2.3.2. Synthesis of Metal Complex

To a stirred methanolic (50 mL, Sigma-Aldrich chemical) solution of ligand, L1 (762 mg, 2.1 mmol), the $CuCl_2 \cdot 2H_2O$ (170 mg, 1.0 mmol) was added with continuous stirring for 30 min. Then sodium diethyldithiocarbamate (172 mg, 1.0 mmol) was added and the reaction continued for 4 h under an inert atmosphere. The precipitation of the metal complex was obtained after an addition of hexane

(55% yield). The product was filtered, washed with hexane and dried in a vacuum. $^{1}$H NMR (400 MHz, DMSO, ppm): δ 11.81 (s, 2H), 8.64 (d, 2H), 8.20 (d, 4H), 7.91 (d, 4H), 7.82 (4H), 7.64 (2H), 7.35 (4H), 7.30 (4H), 6.86 (2H), 5.76 (s, 2H), 3.85 (s, 2H), 3.71 (q, 4H), 3.32 ($H_2O$), 2.49 (DMSO), 1.22 (t, 6H); IR (KBr, $cm^{-1}$): 3420, 3259, 3060, 2977, 1698, 1636, 1560, 1458, 1382, 1346, 1279, 1190, 1152, 1118, 1070, 1011, 850, 886, 748; Elemental analysis calculated as: 65.38% (carbon), 4.87% (hydrogen), 10.07% (nitrogen), 6.59% (Sulphur), 6.57% (oxygen), 6.53% (Cu); Found: 66.27% (carbon), 4.18% (hydrogen), 9.70% (nitrogen), 4.18% (Sulphur), 6.17% (oxygen), 3.6% (Cu).

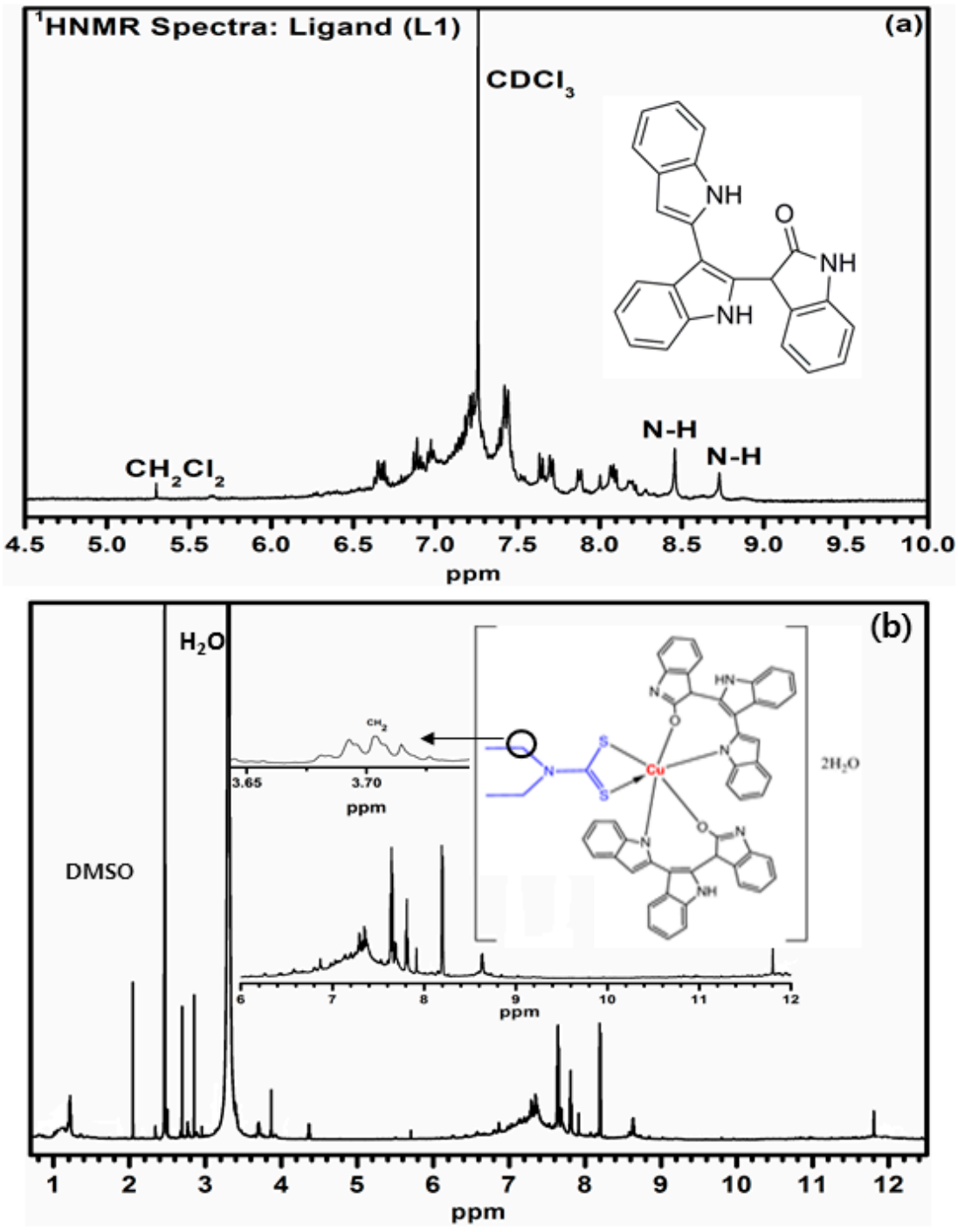


**Figure 1.** $^{1}$HNMR spectra of the (**a**) ligand, L1 and (**b**) mixed ligand Cu (II) complex.

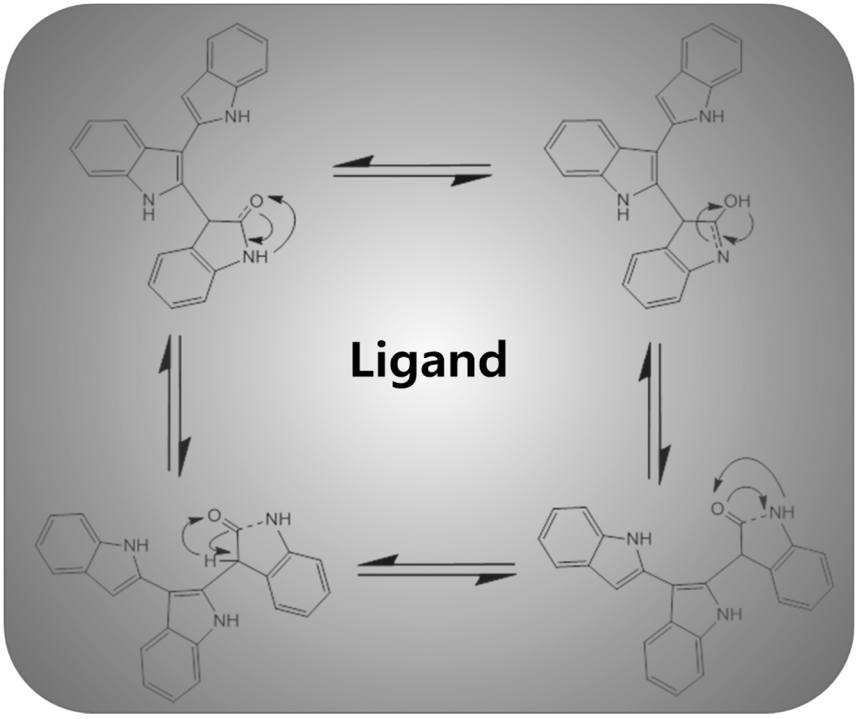


**Scheme 2.** Electron delocalization behavior via keto-enol equilibrium in the synthesized organic ligand (L1).

### *2.4. Detection of Chloride Ions*

An indium tin oxide (ITO) substrate was cleaned and washed with acetone, ethanol and isopropanol followed by drying in an oven. The electrode surface was modified by spin-coating with Cu (II) solution (0.1 M) at 1000 rpm for 30 s and then dried in a vacuum. The as-prepared electrode was applied for electrochemical measurements (cyclic voltammetry) for chloride ion detection by using NaCl (0.1 M) solution in the standard buffer solution (pH = 7) in a three-electrode system.

## 3. Results and Discussion

### *3.1. Spectroscopic Studies of Ligand (L1) Cu (II) Complex*

#### 3.1.1. Nuclear Magnetic Resonance Spectroscopy

$^1$H NMR spectrum (Figure 1a) of the synthesized organic ligand, L1, was observed in deuterated chloroform solvent and showed two singlet peaks at 8.4 ppm and 8.6 ppm, assigned to H–N–C=O cyclic ring. The singlet peak at 5.23 ppm is assigned to the C–H of dichloromethane which was used during the purification of L1. Additionally, the peaks of the aromatic protons of the ligand (L1) were observed in the range 6.67–8.42 ppm, while the doublet peaks appeared at 7.62–8.32 ppm corresponding to various benzene C–H protons. Moreover, the origin of the chemical shift at 8.5 ppm might be associated with the aromatic C–H in position 3 of the indole nucleus. The synthesized organic ligand, L1, exhibits delocalization of electrons through –NH and C=O groups to form tautomeric structures, as shown in Scheme 2. The signal in the range of 0.95–1.2 ppm has been observed for the methyl group of the coordinated diethyldithiocarbamate ligand (L2). The proton NMR spectra (Figure 1b) of mixed-ligand Cu (II) complex was observed in the deuterated dimethyl sulfoxide solvent with TMS as internal reference. The –$CH_2$ protons of the diethyldithiocarbamate moiety is assigned at the 3.7 ppm (quadruplet) of the Cu (II) complex [26]. The O=C–NH proton has been assigned the strong signal at 3.36 ppm while attachment of third benzopyrrole moiety was observed due to the presence of a singlet peak at 4.34 ppm, hence a decrease in the chemical shift in the metal complex as compared to the organic ligand. The chemical shift values of other aromatic protons were observed in the region of

7.32–8.23 ppm for the metal complex alongside the peak at 8.72 and 11.65 ppm corresponding to the –NH proton of the cyclic benzopyrrole moiety [27].

### 3.1.2. Fourier Transforms Infrared Spectroscopy

The FTIR spectra in Figure 2a of the organic ligand (L1) showed a strong stretching band of the secondary amine N–H group in the 3421–3249 $cm^{-1}$ region for both the ligand and the metal complex. The disappearance of the 3495 $cm^{-1}$ peak of the ligand confirms the attachment of the metal with the N–H via coordination bond as the electron delocalization takes place in keto-enol forms of the synthesized organic ligand, L1. The neutral ligand indicates that the proton is bonded to the nitrogen atom instead of the oxygen and exhibits tautomeric structures (Scheme 2) which evidenced that the ketone form is more stable than the hydroxyl form. The peaks in the 3057–2905 $cm^{-1}$ region were assigned to the C–H stretching bands present in the synthesized oxindole-based ligand. The slightly lower shifting of the C=O stretching band of the ligand from 1640 $cm^{-1}$ to 1638 $cm^{-1}$ in the metal complex might be due to the coordination bonding (ligand to metal bond) of the O atom to the Cu ion [28]. The characteristic C=S peak of the dithiocarbamate ligand appeared in the region of 1328 $cm^{-1}$, which shifted to the lower frequency of 1319 $cm^{-1}$ on complexation with metal, indicating the S coordination attachment of the ligand. After complex formation with metal, the C=N stretching peak (Table 1) also decreased to a low frequency from 1569 $cm^{-1}$ to 1556 $cm^{-1}$, suggesting N coordination towards the metal ion. The denticity of various ligands can ascertain the unsymmetrical monodentate or bidentate coordination via IR spectroscopy [29]. The single peak in the frequency region of 1020–950 $cm^{-1}$ implies the bidentate attachment of the dithiocarbamate moiety with the metal ion. Additionally, the presence of a thioureide (N–CSS) peak around 1520 $cm^{-1}$ in the metal complex indicates the presence of adjacent C–S and N–C bonds of the thiocarbamate ligand with a supporting C–S peak in the 1012 $cm^{-1}$ region [30].

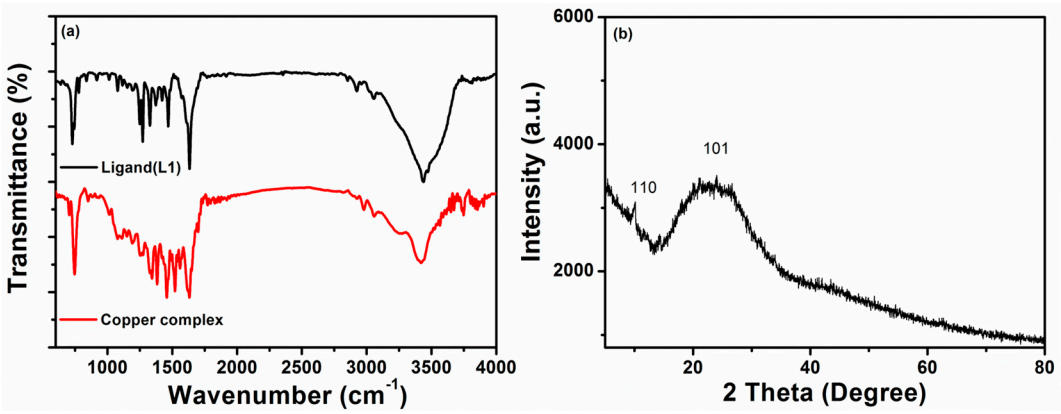


**Figure 2.** (**a**) FTIR spectra of organic ligand (L1) and Cu (II) complex and (**b**) powder XRD plot of mixed ligand Cu (II) complex.

**Table 1.** Characteristic IR bands ($cm^{-1}$) of the organic ligand (L1) and its Cu (II) complex with KBr pellets as reference.

| Compounds | υ(N-H) | υ(C-H) | υ(C=O) | υ(C=N) | υ(C=S) | υ(C-O) | υ(C=C) |
|---|---|---|---|---|---|---|---|
| Ligand(L1) | 3459 | 2865–2964 | 1640 | 1569 | 1328 | 1170 | 1275 |
| $[Cu(L1)_2(L2)]$ | 3249 | 2850–2982 | 1638 | 1556 | 1319 | 1172 | 1266 |

### 3.1.3. Powder X-Ray Diffraction Analysis

XRD spectral study of the Cu (II) complex is shown in Figure 2b. The XRD pattern of the metal complex shows a small peak at 10.13° and a broad peak at 24.02°, indicating that the metal complex has a low crystalline nature and is expected to have a solid amorphous state.

### 3.2. Electronic Properties of Cu (II) Complex

Electronic spectra (Figure 3a) of the ligand (L1) showed two absorption peaks in chloroform. The broad peak around 220–246 might be assigned to the π-π* transition with a sharp peak at 302 nm to the n-π* electronic transitions. For the metal complex, three distinct absorption peaks were obtained in the chloroform solution. The high-intensity peak at 246 nm and a sharp peak at 300 nm corresponded to π-π* transitions and n-π* transition peaks of the organic ligand, which show a slight decrease in wavelength after metal complex formation. Additionally, the peak at 350 nm has been observed for the ligand to metal charge transfer (LMCT) transitions while the broad peak at 420 nm might be assigned to charge transfer transition ($^2E_g \rightarrow {}^2T_{2g}$) due to the Jahn-Teller distortion of the geometry of the Cu (II) complex [31]. The obtained metal complex has shown strong solution stability in DMSO and DMF under the UV–Vis bands for a week. The electronic spectrum of the complex has shown a sharp peak at 217 nm and charge transfer (CT) peak at 293 nm in methanol. The intensity of the CT peak increased upon irradiation by UV light at 25 °C without any other changes in the visible spectra of the Cu (II) complex [32]. The effects of various alcoholic solvents (Figure 3b) on the electronic spectra of the synthesized Cu (II) complex were also studied at the room temperature. Upon increasing the alkyl chain of the corresponding alcohols (ethanol to butanol), the slight blue shift in the peaks (211 and 207, respectively) and red shift in the peaks (295 and 298, respectively) were observed. However, the electronic spectra in isopropanol solution shows a peak at 209 nm and a distinct sharp peak at 297 nm [33].

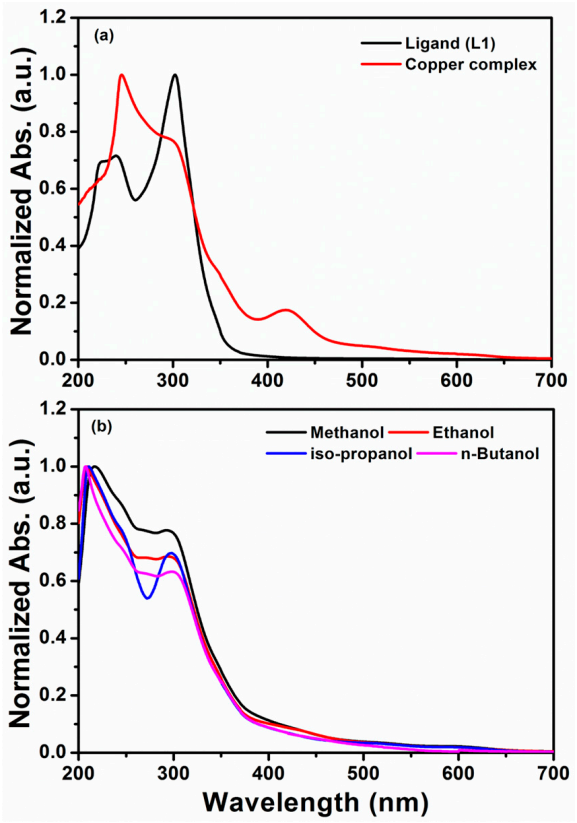


**Figure 3.** (**a**) Electronic spectra of the organic ligand, L1 and Cu (II) complex in chloroform solvent, (**b**) UV-visible spectra of Cu (II) complex in various alcoholic solvents.

### 3.3. Thermal Properties of the Cu (II) Complex

The thermogravimetric analysis (Figure 4a) of Cu (II) complex (empirical formula-$C_{53}H_{44}CuN_7O_4S_2$) reveals the decomposition of water molecules around 115 °C. The Cu (II) complex showed its first decomposition (Scheme 3) around the temperature range of 100–160 °C with 11.12% weight loss which

might be due to the loss of water molecules with the diethyl amine fraction of diethyldithiocarbamate ligand, L2. But the second decomposition of 8.88% weight loss in the temperature range of 160–234 °C occurred owing to the loss of the carbon disulfide ($CS_2$) moiety of the remaining L2 ligand. The third decomposition of 14.61% weight loss was obtained in the temperature range of 240–392 °C, which corresponds to the partial loss of the $C_8H_5N$ moiety of the organic ligand, L1. Finally, the fourth decomposition takes place around the temperature range of 395–465 °C due to the loss of the remaining organic ligand and metal oxide formation with carbon as residue [34]. The observed decompositions conform with the calculated values of Cu (II) complex and its mass percentage-derivative (Figure 4b) during thermal analysis under an inert atmosphere.

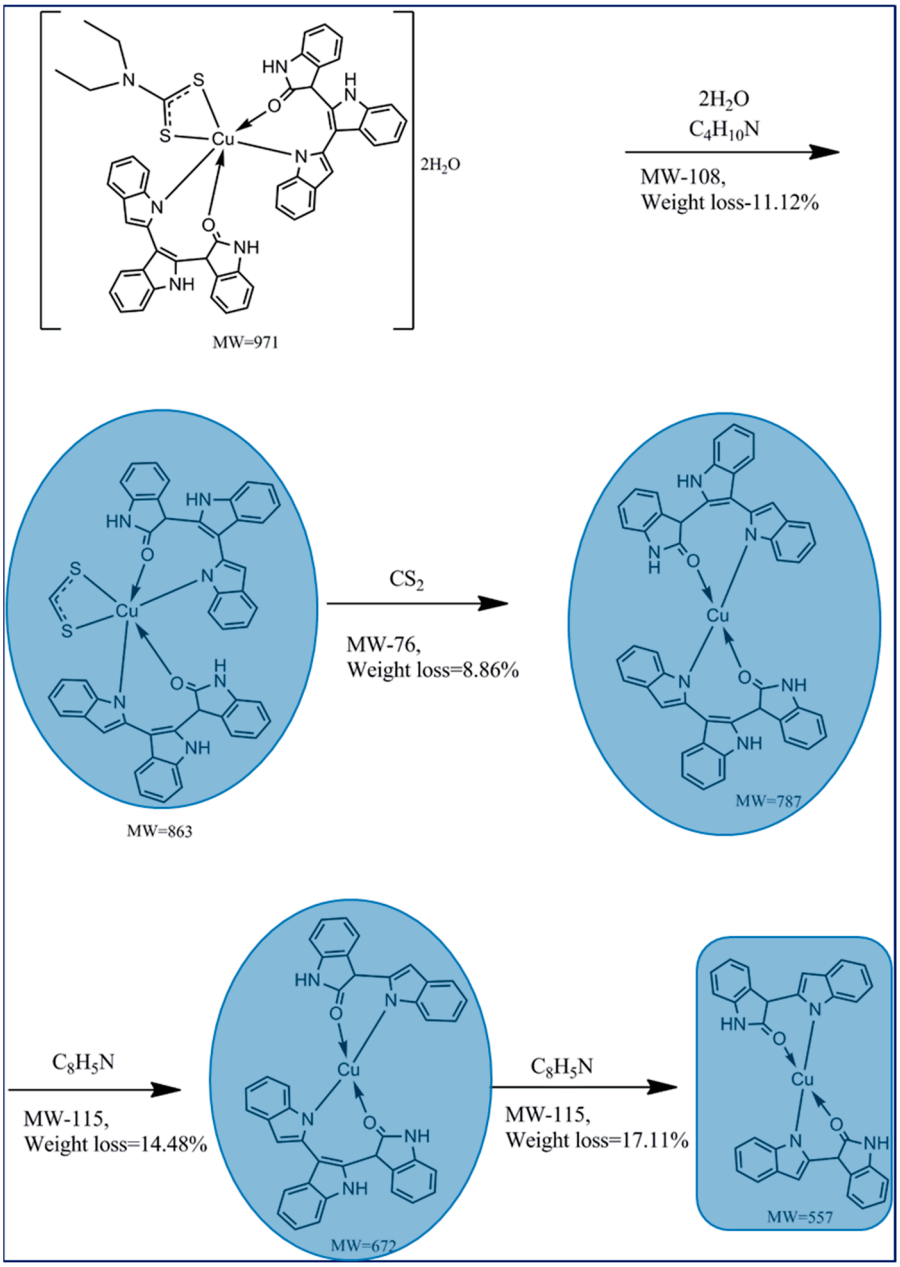


**Scheme 3.** Possible fragmentation pattern of the Cu (II) complex.

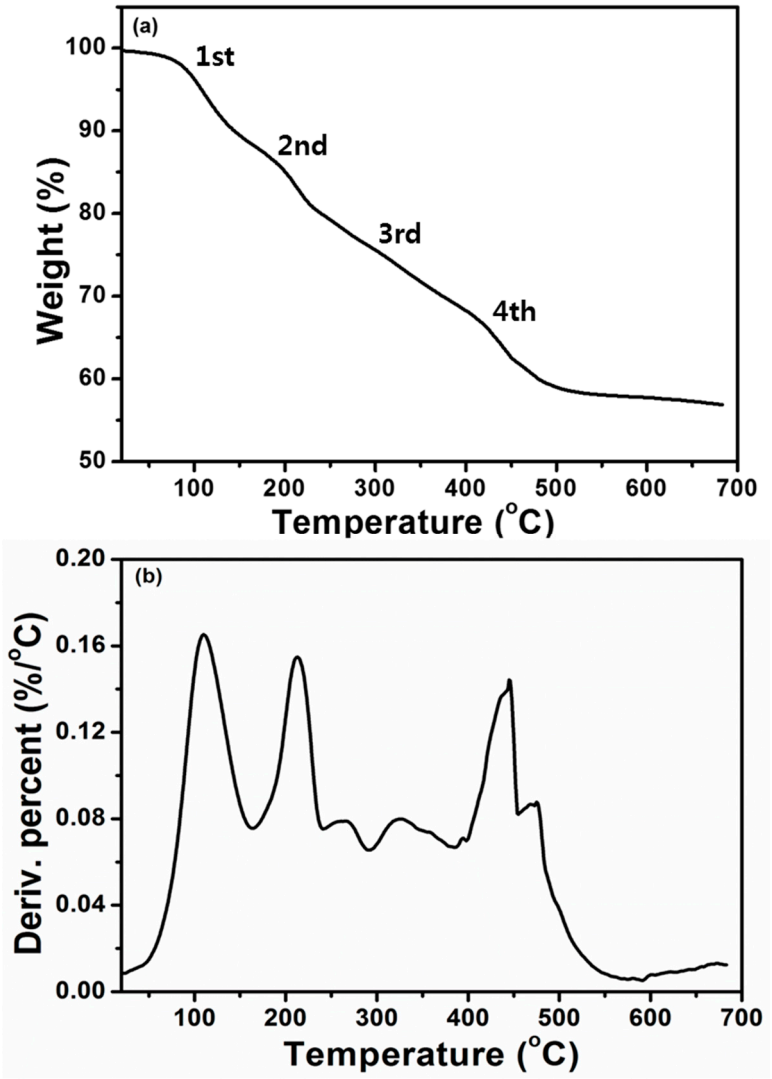


**Figure 4.** (**a**) Thermogravimetric analysis of Cu (II) complex with the scan rate of 10 °C/min under nitrogen, (**b**) percent derivative curve of the Cu (II) complex.

### *3.4. Scanning Electron Microscopic Analysis*

The SEM analysis was used to get the powder images of the Cu (II) complex as shown in Figure 5. The synthesized Cu (II) complex exhibits flower-like structures as observed in the SEM image of Figure 5a. The high-resolution image (Figure 5b) evidenced that the metal complex contains various types of nanoparticles with a micron diameter size. However, small-size nanoparticles are grouped to agglomerates and form large particles as shown in the high-resolution SEM image.

### *3.5. Electrochemical Analysis of Cu (II) Complex*

To explore the electrochemical properties (Figure 6) of the Cu (II) complex, cyclic voltammetry was employed in a three-electrode system. The cyclic voltammograms of Cu (II) complex were recorded at a glassy carbon electrode in $CH_3CN$ containing 0.1 M $TBAPF_6$ as a supporting electrolyte in the potential range from −1.6 V to +1.6 V with a scan rate of 100 mV $s^{-1}$. The Cu (II) complex shows three reduction peaks with Epa values of +0.412, −0.96, and −1.36 V vs. SCE. Hence, the irreversible reduction process of the Cu (II) complex leads to the deposition of Cu (0) on the electrode surface [35]. The peak potential (+0.412 V) might be attributed to the reduction of $Fc^+/Fc$, whereas the peak potential (−1.00 V) can be assigned to the reduction of $Cu^+/Cu$. Additionally, the third reduction potential (−1.36 V) might be ascribed to the Cu(II)/Cu(I) reduction process. During the reverse scan, three oxidation peaks of

−0.64, +0.38, +0.47 V vs. Ag/AgCl were observed. The first peak (Epc −0.64 V) is associated with the oxidation peak of Cu (I)/Cu (II) while the second peak (+0.38 V) is associated with the ligand L1. In addition, the third peak is assigned to the reference redox couple of $Fc/Fc^{+}$ [36].

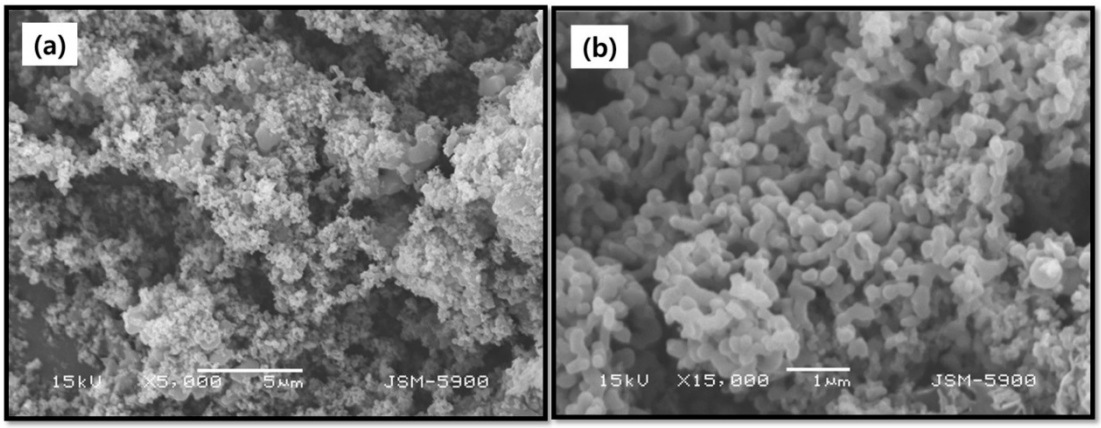


**Figure 5.** SEM images: (**a**) low resolution, and (**b**) high resolution of the mixed ligand Cu (II) complex.

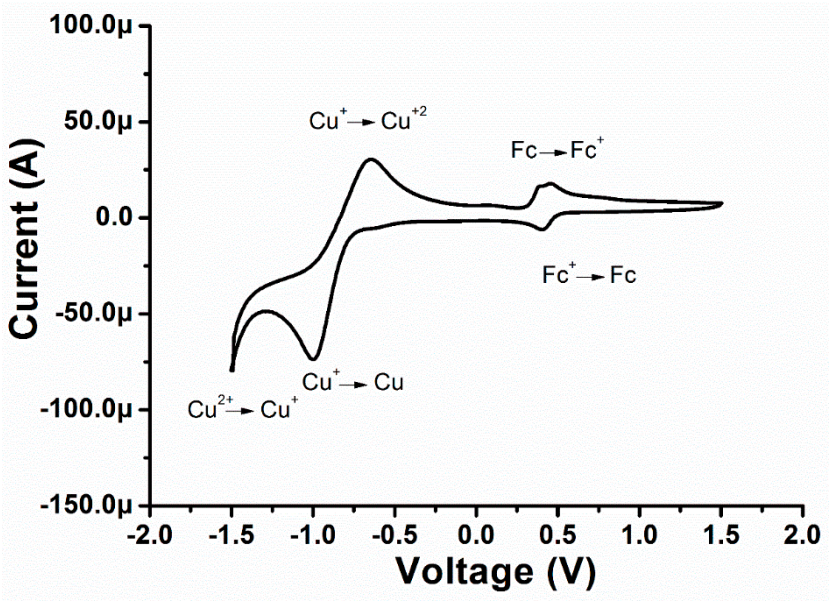


**Figure 6.** Cyclic voltammograms of the Cu (II) complex in $CH_3CN$ (0.1 mol $L^{-1}$ $TBAPF_6$), glassy carbon working electrode, Ag/AgCl reference electrode and platinum wire electrode with scan rate 100 mV $s^{-1}$.

### *3.6. Electrochemical Chloride Ion Detection by the Cu (II) Complex*

For extensive electrochemical application, the prepared mixed Cu (II) complex was used for the detection of chloride ions by adding a fixed amount of NaCl in a standard buffer solution (pH = 7) via cyclic voltammetry (CV). The electrochemical properties of Cu (II) complex were investigated by using the three-electrode system in the potential range from +0.80 V to −0.80 V in a standard buffer (pH = 7) at various scan rates. The CV plots (Figure 7) of Cu (II) complex have shown two peaks in the standard buffer (pH = 7) electrolyte. The cathodic peak was obtained in the forward scan and anodic peak during the reverse scan of CV measurements.

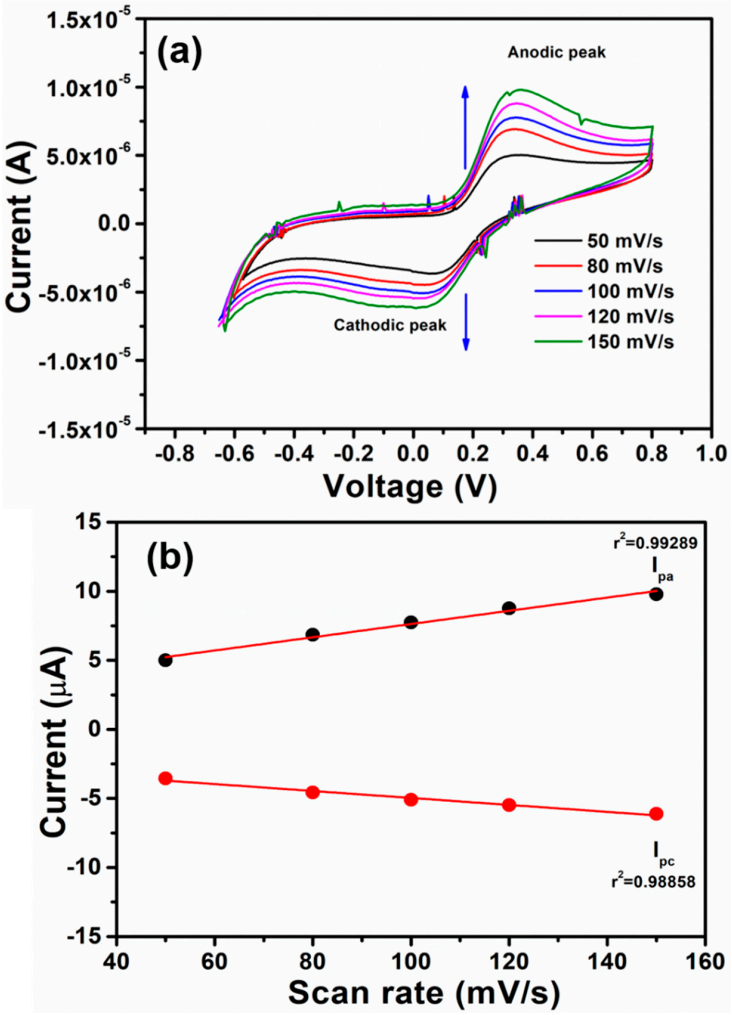


**Figure 7.** (**a**) Cyclic voltammograms of Cu (II) complex in NaCl (0.1M) and phosphate buffer (pH = 7) solution at different scan rate and (**b**) variation of cathodic and anodic current with respect to scan rate.

The cathodic and anodic currents increased with the increase in scan rate from 50 $mVs^{-1}$ to 150 mV/s. Furthermore, the cathodic potential ($E_{pc}$) is shifted towards more negative potentials, and the anodic potential ($E_{pa}$) moved to more positive potentials with increasing scan rates towards the detection of chloride ions [37]. The plot of anodic and cathodic peaks versus scan rates (Figure 7b) has shown a linear dependence relation and hence suggests a quasi-reversible nature and diffusion-controlled transfer of electrons during the electrochemical reaction. The electrochemical system shows excellent retention coefficients ($r^2$) of 0.99246 and 098866, respectively, which again deduces the good detection of chloride ions in neutral buffer electrolytes [38,39].

## 4. Conclusions

The present work reports the synthesis of a novel Cu (II) complex by the reaction of bidentate ligands newly-synthesized oxindole-derivative and dithiocarbamate with hydrated transition metal chloride, $CuCl_2 \cdot 2H_2O$ salts. The Cu (II) complex has shown a distorted octahedral geometry due to the presence of strong Jahn-Teller Distortion resulting in the three electronic transitions. The powder morphology of the Cu (II) complex using SEM analysis showed that the particles were agglomerated and matched elemental compositions. The obtained Cu (II) complex has shown irreversible redox properties with two reduction peaks and good stability in DMSO and DMF solution phases. The mixed Cu (II) complex exhibits the high cathodic and anodic current in chloride containing a neutral buffer, indicating the excellent ability of the complex for the detection of chloride ions.

**Author Contributions:** M.N., A., S.A., M.S.A. and H.-S.S. conceived and designed the experiments; M.N., A. and S.A., performed the experiments, and analyzed the data contributed reagents/materials/analysis tools, wrote and revise the paper.

**Acknowledgments:** Sadia Ameen acknowledges NRF Project#2016R1D1A1B03934446. This work is also supported by NRF Project#2017R1A2B2003381. This paper was supported by research funds for newly appointed professors of Chonbuk National University in 2018.

**Conflicts of Interest:** The authors declare no conflict of interest.

## References

1. Wei, H.L.; Piou, T.; Dufour, J.; Neuville, L.; Zhu, J. Iodo-Carbocyclization of Electron-Deficient Alkenes: Synthesis of Oxindoles and Spirooxindoles. *J. Org. Lett.* **2011**, *13*, 2244–2247. [CrossRef]
2. Wu, T.; Mu, X.; Liu, G. Palladium Catalyzed Oxidative Arylalkylation of Activated Alkenes: Dual C-H Bond Cleavage of an Arene and Acetonitrile. *Angew. Chem. Int. Ed.* **2011**, *50*, 12578–12581. [CrossRef]
3. Qiu, K.; Chen, Y.; Rees, T.W.; Ji, L.; Chao, H. Organelle-targeting metal complexes: From molecular design to bio-applications. *Coord. Chem. Rev.* **2019**, *378*, 66–86. [CrossRef]
4. Borge, V.V.; Patil, R.M. Syntheses and characterization of copper metal complexes prepared from chalcone derivatives. *Microchem. J.* **2019**, *145*, 456–459. [CrossRef]
5. Zhou, F.; Liu, Y.L.; Zhou, J. Catalytic Asymmetric Synthesis of Oxindoles Bearing a Tetrasubstituted Stereocenter at the C-3 Position. *J. Adv. Synth. Catal.* **2010**, *352*, 1381–1407. [CrossRef]
6. Huters, A.D.; Styduhar, E.D.; Garg, N.K. Total syntheses of the elusive welwitindolinones with bicyclo[4.3.1] cores. *Angew. Chem. Int. Ed.* **2012**, *51*, 3758–3765. [CrossRef]
7. Ball-Jones, N.R.; Badillo, J.J.; Franz, A.K. Strategies for the enantioselective synthesis of spirooxindoles. *Org. Biomol. Chem.* **2012**, *10*, 5165–5181. [CrossRef]
8. Dalpozzo, R.; Bartoli, G.; Bencivenni, G. Recent advances in organocatalytic methods for the synthesis of disubstituted 2- and 3-indolinones. *Chem. Soc. Rev.* **2012**, *41*, 7247–7290. [CrossRef]
9. Klein, J.E.; Taylor, M.N.; Eur, R.J.K. Transition Metal Mediated Routes to 3,3 Disubstituted Oxindoles through Anilide Cyclisation. *J. Org. Chem.* **2011**, *2011*, 6821–6841. [CrossRef]
10. Jia, Y.X.; Kundig, E.P. Oxindole synthesis by direct coupling of C($sp^2$)-H and C($sp^3$)-H centers. *Angew. Chem. Int. Ed.* **2009**, *48*, 1636–1639. [CrossRef]
11. Perry, A.; Taylor, R.J.K. Oxindole synthesis by direct C–H, Ar–H coupling. *Chem. Commun.* **2009**, *45*, 3249–3251. [CrossRef]
12. Pugh, D.S.; Klein, J.E.M.N.; Perry, A.; Taylor, R.J.K. Preparation of 3-Alkyl-Oxindoles by Copper(II)-Mediated C-H, Ar-H Coupling Followed by Decarboxyalkylation. *Synlett* **2010**, 934–938. [CrossRef]
13. Klein, J.E.M.N.; Perry, A.; Pugh, D.S.; Taylor, R.J.K. First C−H Activation Route to Oxindoles using Copper Catalysis. *Org. Lett.* **2010**, *12*, 3446–3449. [CrossRef] [PubMed]
14. Ueda, S.; Okada, T.; Nagasawa, H. Oxindole synthesis by palladium-catalysed aromatic C–H alkenylation. *Chem. Commun.* **2010**, *46*, 2462–2464. [CrossRef]
15. Schiffner, J.A.; Oestreich, M. All-Carbon-Substituted Quaternary Carbon Atoms in Oxindoles by an Aerobic Palladium(II)-Catalyzed Ring Closure onto Tri- and Tetrasubstituted Double Bonds. *Eur. J. Org. Chem.* **2011**, *2011*, 1148. [CrossRef]
16. Jaegli, S.; Dufour, J.; Wei, H.I.; Piou, T.; Duan, X.H.; Vors, J.P.; Neuville, L. Palladium-Catalyzed Carbo-Heterofunctionalization of Alkenes for the Synthesis of Oxindoles and Spirooxindoles. *J. Org. Lett.* **2010**, *12*, 4498–4501. [CrossRef]
17. Chauke, V.P.; Antunes, E.; Nyokong, T. Comparative behavior of conjugates of tantalum phthalocyanines with gold nanoparticles or single walled carbon nanotubes towards bisphenol A electrocatalysis. *J. Electroanal. Chem.* **2011**, *661*, 1–7. [CrossRef]
18. Hazra, S.; Majumder, S.; Fleck, M.; Aliaga-Alcalde, N.; Mohanta, S. Synthesis, molecular and supramolecular structures, electrochemistry and magnetic properties of two macrocyclic dicopper(II) complexes: Microporous supramolecular assembly. *Polyhedron* **2009**, *28*, 3707–3714. [CrossRef]
19. Premkumar, J.; Ramaraj, R. Photocatalytic reduction of dioxygen by colloidal semiconductors and macrocyclic cobalt(III) complexes in Nafion and cellulose matrices. *J. Mol. Catal. A Chem.* **1998**, *132*, 21–32. [CrossRef]

20. Anbu, S.; Kandaswamy, M.; Suthakaran, P.; Murugan, V.; Varghese, B. Structural, magnetic, electrochemical, catalytic, DNA binding and cleavage studies of new macrocyclic binuclear copper(II) complexes. *J. Inorg. Biochem.* **2009**, *103*, 401–410. [CrossRef]
21. Singh, A.K.; Saxena, P.; Panwar, A. Manganese(II)-selective PVC membrane electrode based on a pentaazamacrocyclic manganese complex. *Sens. Actuators B Chem.* **2005**, *110*, 377–381. [CrossRef]
22. Sil, A.; Ijeri, V.S.; Srivastava, A.K. Coated-Wire Silver Ion-Selective Electrode Based on Silver Complex of Cyclam. *Anal. Sci.* **2001**, *17*, 477–479. [CrossRef]
23. Kumar, P.; Shim, Y.B. A novel Mg(II)-selective sensor based on 5,10,15,20-tetrakis(2-furyl)-21,23-dithiaporphyrin as an electroactive material. *J. Electroanal. Chem.* **2011**, *661*, 25–30. [CrossRef]
24. Elmosallamy, M.A.F.; Fathy, A.M.; Ghoneim, A.K. Lead(II) Potentiometric Sensor Based on 1,4,8,11Tetrathiacyclotetradecane Neutral Carrier and Lipophilic Additives. *Electroanalysis* **2008**, *20*, 1241–1245. [CrossRef]
25. Li, X.C.; Wang, C.Y.; Wan, Y.; Lai, W.Y.; Zhao, L.; Yin, M.F.; Huang, W. A T-shaped triazatruxene probe for the naked-eye detection of HCl gas with high sensitivity and selectivity. *Chem. Commun.* **2016**, *52*, 2748–2751. [CrossRef] [PubMed]
26. Ramadan, S.; Hambley, T.W.; Kennedy, B.J.; Lay, P.A. NMR Spectroscopic Characterization of Copper(II) and Zinc(II) Complexes of Indomethacin. *Inorg. Chem.* **2004**, *43*, 2943. [CrossRef]
27. Shahzadi, S.; Ali, S.; Fettouhi, M. Synthesis, Spectroscopy, In Vitro Biological Activity and X-ray Structure of (4-Methylpiperidine-dithiocarbamato-S,S′)triphenyltin(IV). *J. Chem. Crystallogr.* **2008**, *38*, 273. [CrossRef]
28. Gudasi, K.B.; Patil, S.A.; Kulkarni, M.V.; Nethaji, M. Transition metal complexes of a potential anticancer quinazoline ligand. *Trans. Met. Chem.* **2009**, *34*, 325. [CrossRef]
29. Fuentes-Martinez, J.P.; Toledo-Martinez, I.; Roman-Bravo, P.; Garcia, P.G.; Godoy-Alcantar, C.; Lopez-Cardoso, M.; Morales-Rojas, H. Diorganotin(IV) dithiocarbamate complexes as chromogenic sensors of anion binding. *Polyhedron* **2009**, *28*, 3953–3966. [CrossRef]
30. Tiekink, E.R.T. Tin dithiocarbamates: Applications and structures. *Appl. Organomet. Chem.* **2008**, *22*, 533–550. [CrossRef]
31. Mohamed, G.G. Synthesis, characterization and biological activity of bis(phenylimine) Schiff base ligands and their metal complexes. *Spectrochim. Acta A* **2006**, *64*, 188–195. [CrossRef]
32. Gup, R.; Giziroglu, E. Metal complexes and solvent extraction properties of isonitrosoacetophenone 2-aminobenzoylhydrazone. *Spectrochim. Acta A* **2006**, *65*, 719–726. [CrossRef]
33. Gatto, C.C.; Lang, E.S.; Burrow, R.A.; Abram, U. Syntheses and Structures of 2-Acetylpyridine-(2-amino-benzoylhydrazone) and its Dioxouranium(VI) Complex. *J. Braz. Chem. Soc.* **2006**, *17*, 1612–1616. [CrossRef]
34. Wong, W.W.H.; Curiel, D.; Lai, S.W.; Drew, M.G.B.; Beer, P.D. Ditopic redox-active polyferrocenyl zinc(II) dithiocarbamate macrocyclic receptors: Synthesis, coordination and electrochemical recognition properties. *Dalton Trans.* **2005**, 774–781. [CrossRef] [PubMed]
35. Golcu, A.; Tumer, M.; Demirelli, H.; Wheatley, R.A. Cd(II) and Cu(II) complexes of polydentate Schiff base ligands: Synthesis, characterization, properties and biological activity. *Inorg. Chim. Acta* **2005**, *358*, 1785–1797. [CrossRef]
36. John, R.P.; Sreekanth, A.; Rajakannan, V.; Ajith, T.A.; Kurup, M.R.P. New copper(II) complexes of 2-hydroxyacetophenone N(4)-substituted thiosemicarbazones and polypyridyl co-ligands: Structural, electrochemical and antimicrobial studies. *Polyhedron* **2004**, *23*, 2549–2559. [CrossRef]
37. Shamsipur, M.; Roushani, M.; Pourmortazavi, S.M.; Shahabadi, N. Amperometric determination of sulfide ion by glassy carbon electrode modified with multiwall carbon nanotubes and copper (II) phenanthroline complex. *Cent. Eur. J. Chem.* **2014**, *12*, 1091–1099. [CrossRef]
38. Ramar, V.; Balaya, P. Enhancing the electrochemical kinetics of high voltage olivine LiMnPO4 by isovalent co-doping. *Phys. Chem. Chem. Phys.* **2013**, *15*, 17240–17249. [CrossRef] [PubMed]
39. Li, L.; Tang, X.; Liu, H.; Qu, Y.; Lu, Z. Morphological solution for enhancement of electrochemical kinetic performance of $LiFePO_4$. *Electrochim. Acta* **2010**, *56*, 995–999. [CrossRef]